JCTC Journal of Chemical Theory and Computation

pubs.acs.org/JCTC Article

Employing Pseudopotentials to Tackle Excited-State Electron Spill-Out in Frozen Density Embedding Calculations

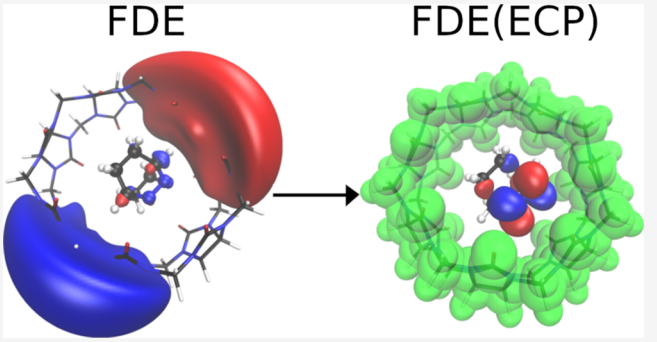
Robert S. Treß,* Christof Hättig, and Sebastian Höfener*

Cite This: J. Chem. Theory Comput. 2022, 18, 1737−1747 Read Online

ACCESS | Metrics & More | Article Recommendations | Supporting Information

Downloaded via BOCHUM LIBRARIES on March 4, 2023 at 14:10:28 (UTC).
See https://pubs.acs.org/sharingguidelines for options on how to legitimately share published articles.

ABSTRACT: In frozen density embedding (FDE), the properties of a target molecule are computed in the presence of an effective embedding potential, which accounts for the attractive and repulsive contributions of the environment. The formally exact embedding potential, however, is in practice calculated using explicit kinetic-energy functionals for which the resulting potentials are in many cases not repulsive enough to account fully for Pauli repulsion by the electrons of the environment and to compensate thereby the strong electron−nuclear attraction. For the excited states on the target molecule, this leads to charge spill-out when diffuse basis functions are included, which allow that valence electrons are excited to those regions of the environment where the strong nuclear attraction is not sufficiently compensated by repulsive contributions. To reduce this insufficiency, we propose in the present work the inclusion of atomic all-electron pseudopotentials for all environment atoms on top of the conventional embedding potential. In the current work, the pseudopotentials are applied for computing vertical excitation energies of local excited states in complex systems employing the second-order algebraic diagrammatic construction (ADC(2)) scheme. The proposed approach leads to significantly reduced charge spill-out and an improved agreement of FDE and supermolecular calculations in the frozen solvent approximation. In particular, when diffuse functions are employed, the mean absolute deviation (MAD) is reduced from 0.27 to 0.05 eV for the investigated cases.



1. INTRODUCTION

One of the everlasting problems of quantum chemistry is the large increase of computation time with system size, making the calculation of large biomolecules or complex systems very expensive or even impossible tasks. One way to decrease the computation time of complex systems are embedding methods, where the focus is set to only a part of the system and the influence of the environment onto this part is approximated. A popular class of embedding methods are QM/MM methods,[1−5] where the environment is described through point charges and force field methods. One representative is the polarizable embedding[6] (PE) method. Here, the polarization of the MM region is additionally taken into account through point dipole−dipole polarizabilities, fluctuating charges, or Drude oscillators.

A problem of QM/MM methods is that they miss purely quantum mechanical interactions without classical counterparts such as Pauli repulsion and nonadditive energy contributions that become important when the electron densities of the active part and the environment start to overlap. For this task, a quantum mechanical description of the environment is needed, also denoted as QM/QM embedding. One method belonging to this class is frozen density embedding (FDE).[7] In FDE, the total system is divided into small quantum mechanically described subsystems, and the interaction between them is expressed through density functional theory (DFT). While FDE was developed in the framework of DFT, it was combined with wave function-based methods already in the 1990s.[8,9] Recently, it has been extended to methods suitable for dynamic correlation and excited states.[10−14] A response theory formulation within FDE was first proposed for three overlapping partitions in 2004[15] and later extended to a general subsystem DFT response approach, also denoted as coupled FDE (FDEc).[16,17]

While the FDE approach is formally exact, in practice approximations similar to DFT must be made, including the use of approximate functionals in the interaction term, which for example are not able to capture long-range dispersion effects.[18] Additionally, the interaction term requires an explicit approximate semilocal kinetic-energy functional. The latter is an important repulsive contribution, in particular close to the nuclei of the environment where the strong Coulomb

Received: July 21, 2021
Published: February 2, 2022



ACS Publications
© 2022 The Authors. Published by American Chemical Society

https://doi.org/10.1021/acs.jctc.1c00732
J. Chem. Theory Comput. 2022, 18, 1737−1747

attraction has to be compensated to prevent electron spill-out from the active subsystem into these regions.[19,20]

In the present work, furthermore the uncoupled (FDEu) scheme using the monomer basis is applied to avoid computational steps that involve the whole supermolecular system and thereby provides a route for calculations on much larger systems. While the coupled FDEc treatment enables one to treat excited states extending to environment subsystems, in the FDEu approximation used in the current work only excited states localized on one subsystem are accessible.

The missing Pauli repulsion originating from the orthogonality condition is with numerically accurate implementations usually not a problem for electronic ground states[21] but can still cause severe problems for excitation energies,[22,23] especially in combination with diffuse basis functions that are often essential for obtaining the excited state accurately. In such cases, it can change the energetic order of the excited states and induce low-lying artificial charge-transfer states, that is, an excited-state electron spill-out problem. One way to improve the repulsion is through embedding potential corrections such as long-distance corrections for the kinetic-energy component[24] or an energy correction[25] similar to the DFT-D[26,27] approach for dispersion. The orthogonality of the orbitals between the subsystems can be restored with projection-based embedding.[28−31] A first derivation of subsystem TDDFT with projection-based embedding has been reported in ref 32. However, in this work wrong assumptions were made, but refs 33−36 have shown that supermolecular excitation energies and properties can be restored if coupling matrix contributions are correctly taken into account. Because of the orthogonalization for the whole supersystem, however, these approaches come at a comparatively high computational cost. The description by the embedding potential can also be improved through the potential reconstruction scheme,[37] leading to improvements in TDDFT excitation energies of systems with hydrogen-bonding interactions.[38] However, the necessary supermolecular calculations make this method quite expensive for large environments.

We aim to address the problem of missing Pauli repulsion by reintroducing it into the embedding potential through effective core potentials, following the strategy of ref 39 used for PE, resulting in a significant improvement in the accuracy of excitation energies within the Algebraic Diagrammatic Construction through the second-order, ADC(2), model.[40−42] Effective core potentials (ECP) come with a small cost and are already implemented in many quantum chemical programs. Using ECPs to model chemically inactive electrons is a well-known approach and commonly used for heavy elements to replace inner electrons and to model the most important relativistic effects in otherwise nonrelativistic calculations.[43] In combination with embedding methods, ECPs have first been used to model cations in embedded cluster calculations to analyze defects in ionic crystals.[19,44] In particular, in the latter context, the idea of representing less important parts of the system by model potentials has also been extended to include valence electrons, for example, in the (fragment) ab initio model potential approach of Seijo and coworkers.[45,46] Similar ideas are also used to represent atoms or functional groups at the QM−MM boundary in QM/MM approaches.[47−50]

Because FDE does not use point charges and multipoles to approximate the embedding potential and includes repulsive contributions originating from the exchange and kinetic energy, missing intersystem Pauli repulsion is for ground-state FDE calculations less an issue[21] than for the QM/MM approaches mentioned above. Probably for this reason, ECPs have to the best of our knowledge until now not been used for the computation of excitation energies within the FDEu model, although the missing intersystem Pauli repulsion is much more important for excited states where energetically higher-lying orbitals are occupied, which are either themselves more diffuse than those occupied in the ground state or are energetically close to such diffuse orbitals. In the current work, we assess the performance of ECPs fitted to reproduce the virtual orbital energies of noble gases atoms for mitigating the problems from missing Pauli repulsion for FDEu at the level of ADC(2) as the correlated wave function method to compute excitation energies within the frozen solvent approximation,[51] that is, neglecting the response of the solvent. The latter allows one to compare the FDE results directly with those from ADC(2) calculations that use a supermolecular Hartree−Fock reference but allow only excitations out of orbitals located on the active subsystem. Besides the general performance of the approach, an important question will be whether including such ECPs simultaneously with the nonadditive kinetic and exchange energy contributions, that are part of the FDE scheme, will lead to double counting of repulsive interactions.

2. THEORY

Frozen density embedding (FDE) as used in combination with wave function methods goes back to subsystem DFT, in which the total density of a system is decomposed into the subsystem densities:

$$\rho(\mathbf{r}) = \sum_{i=1}^{m} \rho_i(\mathbf{r}) \tag{1}$$

where m denotes the number of subsystems, typically corresponding to the number of molecules. On the basis of this decomposition of the density, the energy of the total system is written as the sum of the energy contributions of the individual m subsystems plus one interaction contribution, expressed using the densities of the subsystems:

$$E_{\text{tot}} = \sum_{i=1}^{m} E_i[\rho_i(\mathbf{r})] + E_{\text{int}}[\rho_1(\mathbf{r}), ..., \rho_m(\mathbf{r})] \tag{2}$$

Formally, the interaction energy is defined therefore as the difference between the individual energies and the total energy:

$$E_{\text{int}}[\rho_1(\mathbf{r}), ..., \rho_m(\mathbf{r})] = E_{\text{tot}}[\rho_1(\mathbf{r}), ..., \rho_m(\mathbf{r})] - \sum_{i=1}^{m} E_i[\rho_i(\mathbf{r})] \tag{3}$$

The main advantage of the decomposition and sorting is rooted in the description of the interaction term as a functional of the subsystem densities, as the decomposition allows for employing different methods for the individual subsystems in general and the use of wave function methods in particular. If wave function methods are used, for example, for all subsystems, one can replace the density functional for the energy of these individual subsystems in eq 2 with a functional of the wave function. Note, however, that the interaction contribution is nevertheless expressed in terms of the subsystem densities; see eq 3:

https://doi.org/10.1021/acs.jctc.1c00732
J. Chem. Theory Comput. 2022, 18, 1737−1747

$$E_{\text{tot}} = \sum_{i=1}^{m} E_i[\Psi_i(\mathbf{r})] + E_{\text{int}}[\rho_1(\mathbf{r}), ..., \rho_m(\mathbf{r})] \tag{4}$$

The motivation for this is that the interaction energy can then be expressed in terms of the densities, independent of the methods chosen for the individual subsystems:

$$E_{\text{int}}[\rho_1(\mathbf{r}), \rho_2(\mathbf{r}), ..., \rho_m(\mathbf{r})] = -\sum_{i}^{m}\sum_{j\neq i}^{m} \int \rho_i(\mathbf{r}) \nu_j^{\text{N}}(\mathbf{r})\, \mathrm{d}\mathbf{r} + \sum_{i}^{m}\sum_{j\neq i}^{m} \int\int \frac{\rho_i(\mathbf{r})\rho_j(\mathbf{r}')}{|\mathbf{r}-\mathbf{r}'|}\, \mathrm{d}\mathbf{r}\, \mathrm{d}\mathbf{r}' + E_{\text{kxc}}^{\text{nadd}}[\rho_1(\mathbf{r}), ..., \rho_m(\mathbf{r})] + E_{\text{NN}} \tag{5}$$

where ν_j^{N} is the potential of the nuclei of subsystem j. $E_{\text{kxc}}^{\text{nadd}}$ contains the nonadditive contributions of the kinetic and exchange-correlation energy and is given as

$$E_{\text{kxc}}^{\text{nadd}}[\rho_1(\mathbf{r}), ..., \rho_m(\mathbf{r})] = T[\rho_1(\mathbf{r}) + ... + \rho_m(\mathbf{r})] - \sum_{i}^{m} T^i[\rho_i(\mathbf{r})] + E_{\text{xc}}[\rho_1(\mathbf{r}) + ... + \rho_m(\mathbf{r})] - \sum_{i}^{m} E_{\text{xc}}^i[\rho_i(\mathbf{r})] \tag{6}$$

Note that the kinetic contributions need to be computed using an explicit, that is, approximate, kinetic-energy functional. Deriving equations for the energy, or wave function, of a subsystem i leads to the conventional equations for the energy, or wave function, of a subsystem, which in the embedding case contains additional terms due to the interaction energy. These additional terms based on the interaction energy are commonly denoted as embedding potential and are given by

$$\nu_{\text{emb}}^i(\mathbf{r}) = -\sum_{j\neq i}^{m} \nu_j^{\text{N}}(\mathbf{r}) + \sum_{j\neq i}^{m} \int \frac{\rho_j(\mathbf{r}')}{|\mathbf{r}-\mathbf{r}'|}\, \mathrm{d}\mathbf{r}' + \nu_{\text{kxc}}^i(\mathbf{r}) \tag{7}$$

where ν_{kxc}^i contains the nonadditive contributions obtained as the functional derivative:

$$\nu_{\text{kxc}}^i(\mathbf{r}) = \left.\frac{\delta(T[\rho]+E_{\text{xc}}[\rho])}{\delta\rho}\right|_{\rho=\rho_{\text{tot}}} - \left.\frac{\delta(T[\rho]+E_{\text{xc}}[\rho])}{\delta\rho}\right|_{\rho=\rho_i} \tag{8}$$

The embedding potential given in eq 7 is used in the present work in ground-state Hartree−Fock, ground-state second-order Møller−Plesset perturbation theory (MP2), as well as the response equations for the second-order adiabatic-diagrammatic construction (ADC(2)) scheme by including it in the Fock operator of subsystem i:

$$\hat{F}^{\text{FDE}} = \hat{F}^{\text{vac}} + \nu_{\text{emb}}^i(\mathbf{r}) \tag{9}$$

where $\hat{F}^{\text{vac}}$ is the conventional vacuum Fock operator. No additional changes to the code are needed for MP2 within the perturbation on energy[52] (PTE) reaction field scheme and for ADC(2) if used within the frozen solvent approximation.[51]

Intermolecular interactions can be decomposed into different contributions, see ref 53, of which one important contribution is the repulsive exchange (Pauli) repulsion between the electrons of two fragments having the same spin. Note, of course, that only the total intermolecular interaction is an observable, but the individual contributions are not. For example, if the exchange repulsion is not included as, for example, in mixed quantum-mechanics/molecular mechanics (QM/MM) methods, attractive contributions might dominate too strongly so that the intersystem distance of two fragments is too short. On the basis of this analysis, effective core potentials were introduced in polarizable embedding.[39]

In FDE, repulsive effects beyond the pure electrostatic contributions are included via the nonadditive exchange-correlation and kinetic terms contained in the embedding potential; see eq 7.[22] The literature reveals, however, that the contributions beyond the pure electrostatic embedding are not large enough in case of strong interactions; for example, in case of potential-energy surfaces, FDE is not repulsive enough.[25] Furthermore, for weakly interacting complexes, an "electron-leak" problem in FDE calculations occurs due to the strongly attractive nuclear potential, which is not compensated sufficiently by the kinetic functional.[24,54] This drawback might be rooted in the approximate kinetic-energy functionals.[20] As a solution, however, the use of effective core potentials was proposed.[19] To the best of our knowledge, ECPs were only pursued in FDE in terms of core orbitals relevant for electronic ground states.

In the present work, we focus on charge spill-out during electronic excitations. If diffuse basis functions are included, which is often necessary for accurate excitation energies, electronic excitations might lead to a charge redistribution such that electron density is moved to environment regions that exhibit a strong nuclear attraction where the repulsion is not sufficiently accounted for by the potential ν_{kxc}^i. The resulting unphysical attraction is significantly reduced when all-electron ECPs are introduced to model the Pauli repulsion, which leads to an improved description of the interaction in particular in regions that are close to nuclei. We therefore add the potential from all-electron ECPs on all atoms in the environment $\hat{\nu}_{\text{ECP}}^i$ to the FDE Fock operator of subsystem i, leading to

$$\hat{F}^{\text{FDE(ECP)}} = \hat{F}^{\text{FDE}} + \hat{\nu}_{\text{ECP}}^i \tag{10}$$

In difference to the local potential $\nu_{\text{kxc}}^i(\mathbf{r})$, the ECP potential $\hat{\nu}_{\text{ECP}}^i$ is nonlocal as it employs projection operators to act on specific parts of the one-electron Hilbert space. This facilitates the modeling of repulsion effects from the Pauli exclusion principle. Using all-electron pseudopotentials instead of effective core potentials that model only core orbitals leads to a description of the Pauli repulsion with all electrons of the environment and not just those near the nuclei. This is very important because the nonbonded interactions between subsystems are expected to happen primarily between valence electrons. A simple set of all-electron pseudopotentials that reproduces the virtual orbital energies of the noble gases and can be used for the elements in the same period has been developed for He, Ne, and Ar in ref 39 and for Kr and Xe in the current work (vide infra). These all-electron pseudopotentials are expected to model approximately the interaction with the valence region of an atom in a molecule if it can be assumed that (for main group elements) the octet rule is fulfilled, which should be the case if the environment has no low-lying electronically excited states. For a given angular momentum, these pseudopotentials include all components and not only selected contributions. Therefore, they are no

https://doi.org/10.1021/acs.jctc.1c00732
J. Chem. Theory Comput. 2022, 18, 1737−1747

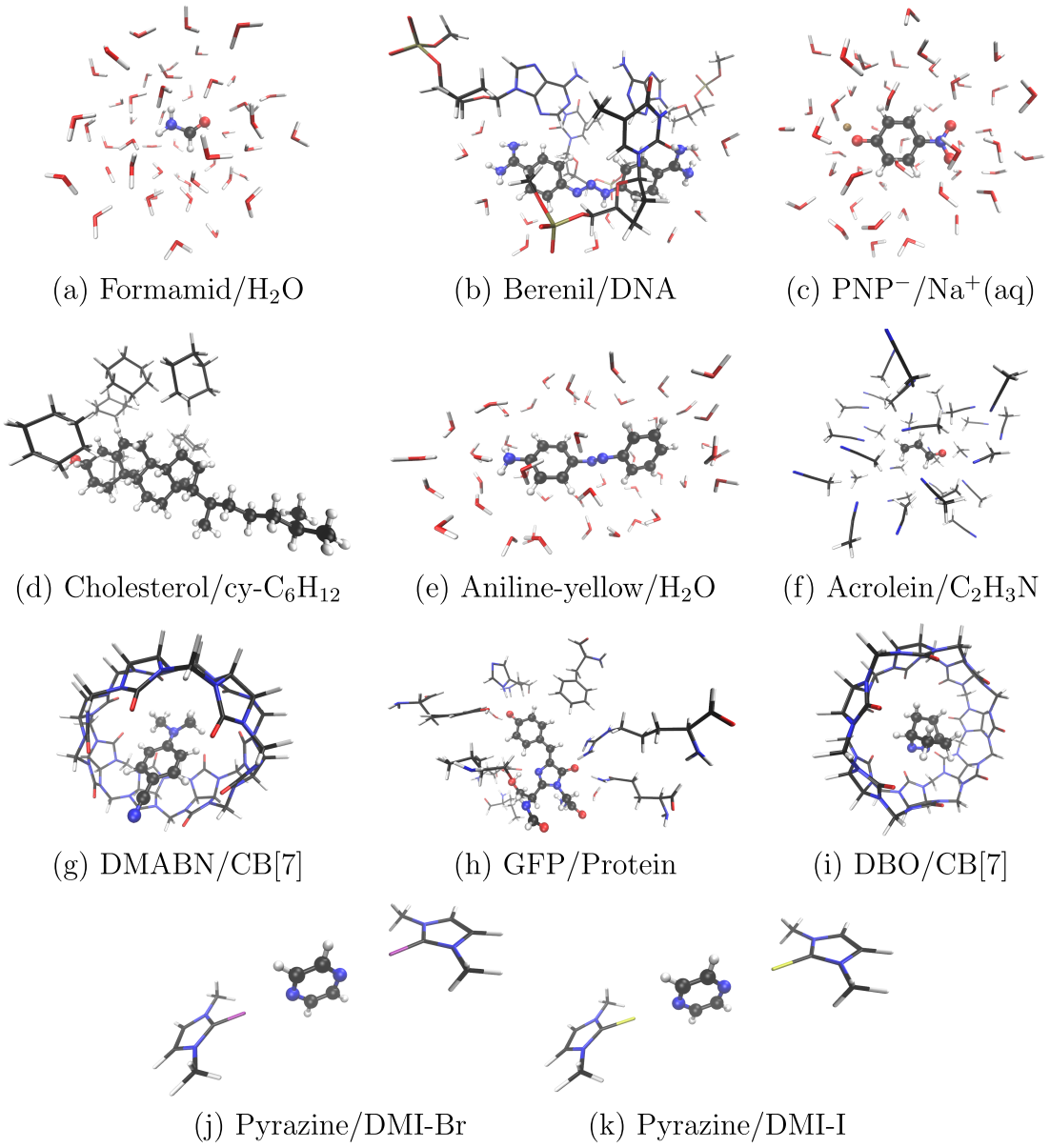


Figure 1. Active/environment total structures of the systems used as a test set. The analyzed chromophore is displayed with balls and sticks, while the environment is displayed as licorice. Systems (a)−(i) are taken from ref 39, while systems (j) and (k) have been constructed in the present work.

longer effective core potentials, but can still be calculated with the available ECP subroutines without further manipulation. To highlight the nature of their computation, we will continue to use the shorthand notation ECP, even though they refer to more than just the core orbitals.

In the FDE approach, the densities of all subsystems are kept frozen except for the active subsystem whose density or wave function is relaxed in the presence of the frozen environment. Subsequently, the role of the active subsystem is shifted to the next subsystem and its density or wave function is optimized accordingly. This is repeated for every subsystem. One cycle in which all subsystems had once the role of the active system is denoted one "Freeze-and-Thaw" (FaT) cycle. The FaT cycles can be repeated until self-consistent convergence for the total system is obtained.

This leads to the following computational protocol for a FDE procedure with m subsystems:

(1) Optimize isolated subsystem densities and save these densities and their electrostatic potentials.

(2) Start the current Freeze-and-Thaw (FaT) cycle using i = 1:

(a) Freeze all subsystems except subsystem i.

(b) Relax the density of the active subsystem i in the presence of the relaxed embedding potential.

(c) Save the density and electrostatic potential of subsytem i.

(d) If $i = m$ exit; otherwise, set $i = i + 1$ and go to step (2a).

(3) If the solution is (within a preset threshold) self-consistent, proceed with step (4); otherwise go to step (2).

(4) Compute the target properties, for example, ADC(2) excitation energies, of the desired subsystems.

While in supermolecular calculations electronic excitations are possibly delocalized over many atoms, FDEu constrains electronic excitations by construction to one subsystem. This

https://doi.org/10.1021/acs.jctc.1c00732
J. Chem. Theory Comput. 2022, 18, 1737−1747

qualitative difference leads to quantitative differences when the comparison of FDE and supermolecular reference results is sought. To provide reference results that are obtained in a spirit similar to FDE, we have implemented the frozen solvent ADC(2) scheme, employing the PNO-ADC(2) code,[55] which uses localized molecular orbitals (LMOs) for the occupied space. In this scheme, the ground-state first-order amplitudes and the excited-state response vectors are restricted to single and double excitations out of LMOs localized on those atoms belonging to the target subsystem in the FDE calculation. In the following, this scheme will be denoted as subsystem-ADC(2).

3. COMPUTATIONAL DETAILS

All calculations in this work were carried out with a local development version of the TURBOMOLE[56] program package. The FDE calculations were performed in the monomer basis of each subsystem. For the embedding potential, the PBE[57] exchange-correlation and the LC94[58] kinetic functional were used together with a supersystem integration grid created from the atomic integration grids of all atoms using grid size 3. We continued with FaT cycles until the electronic energies of all subsystems were converged within a threshold of 5.0×10^{-6} H. Subsequently, excitation energies were computed using the ADC(2) method in the frozen core approximation and the frozen solvent scheme,[51] that is, skipping the response of the environment.

For the atoms H−Ar, we used the all-electron pseudopotentials for He, Ne, and Ar reported in ref 39. For iodine and bromine, we used the all-electron pseudopotentials optimized for krypton and xenon as part of the present work. Details can be found in the Supporting Information. FDE calculations with the pseudopotentials are denoted as FDE(ECP) in the following.

Reference results are computed using the subsystem-ADC(2) approach with a tight PNO truncation threshold of 10^{-9}, using IBO localization. All ADC(2) calculations employed the frozen core approximation for all orbitals with energy below −3 hartree.

3.1. Ethylene−Tetrafluoroethylene Dimer. The geometries of the two molecules ethylene and tetrafluoroethylene (TFE) have been optimized independently of each other with DFT/B3LYP[59] employing D_{2h} symmetry each. These two monomers were then placed coplanar on top of each other, for which the lowest 10 excitation energies have been computed using ADC(2) for distances between 5.5 and 18 bohr. For this system, we used the d-aug-cc-pVTZ basis set,[60] and the densities in the FDE calculations were computed at the Hartree−Fock level of theory.

3.2. Embedding Test Set. For a more representative analysis of the FDE(ECP) approach for excitation energies, we employ a test set consisting of 11 systems; see Figure 1. The structures of systems (a)−(i) were taken from ref 39. These systems contain chromophores in different chemical environments such as water, organic solvents, biomolecular matrixes, and molecular container. They have furthermore been shown to be sensitive to electron spill-out in QM/MM excitation studies. To this set were added systems (j) and (k) to include test cases for bromine and iodine as examples for atoms from periods 4 and 5. The structures for these two systems were optimized using DFT/B3LYP[59] with a grid size of 3 and the cc-pVTZ[61] basis set for the pyrazine subsystem and cc-pVDZ for its environment. This test set allows one to investigate the robustness of the FDE method against electron spill-out and the efficiency of the FDE(ECP) approach in various environments.

The first two vertical excitation energies of the chromophores in the presence of the environment have been computed using the Dunning's cc-pVTZ and aug-cc-pVTZ[62] basis sets for the chromophore and the cc-pVDZ basis set for the environment. For FDE calculations, the HF density was used for the chromophore and the DFT/PBE density employing grid 3 for the environment subsystems. System (h) and (i) have also been computed employing the revapbek[63] and Thomas−Fermi kinetic functional[64,65] for the embedding potential. The results can be found in the Supporting Information. Because the difference in excitation energies between the investigated kinetic energies is comparably smaller than the difference from the reference, they are not discussed further. As in ref 39, for system (h), only the first excitation energy is included.

The potentials for the PE and PE(ECP) calculations were taken for systems (a)−(i) from ref 39. For system (j) and (k), we used a IAO-D3 potential; that is, multipole moments are obtained from an IAO analysis of each subsystem, and the polarizabilities are taken from the DFT-D3 correction parameters.[27] Excitation energies were computed neglecting the response of the environment and using the frozen core approximation.

Subsystem-ADC(2) excitation energies of systems (h) and (i) were also computed with different localization methods, for example, the Boys[66,67] method, the second moment[68] method with an exponent of 2, and the fourth moment[69] method; see the Supporting Information. The different localization methods result in only insignificant changes in the excitation energies and will not be discussed further.

4. RESULTS

4.1. Ethylene−TFE Dimer. We have used the ethylene−TFE dimer to study the effect of different contributions from the intermolecular interaction on excitation energies as a function of the interaction strength, which for this system can easily be tuned by changing the distance between the molecules. The different effects from the ground-state potential (without London dispersion) and the remaining contributions as excitonic coupling and excited-state response on the interaction-induced shift of the excitation energies can be seen in Figure 2, which shows the first eight excitation energies of the ethylene−TFE dimer from supermolecular and subsystem-ADC(2) calculations. One can see that at large distances for all eight excitations the results obtained with the two approaches converge to the same values, as it should be as long as none of the excited states is a long-range charge-transfer state that would be missing in the subsystem-ADC(2) calculations. If the two molecules get closer, the differences between both approaches increase. Major differences are in particular seen for the higher lying states and at short distances (below about 7.086 bohr). A big effect can be seen in the third excitation energy where both approaches end up with a difference of 1.52 eV at a distance of 5.5 bohr. This illustrates that supermolecular calculations are not a helpful reference for validating the accuracy of individual contributions of uncoupled embedding approaches for excitation energies.

Figure 3a and b shows the first four excitation energies of, respectively, the ethylene and TFE subsystems within the ethylene−TFE dimer employing FDE, FDE(ECP), and

https://doi.org/10.1021/acs.jctc.1c00732
J. Chem. Theory Comput. 2022, 18, 1737−1747

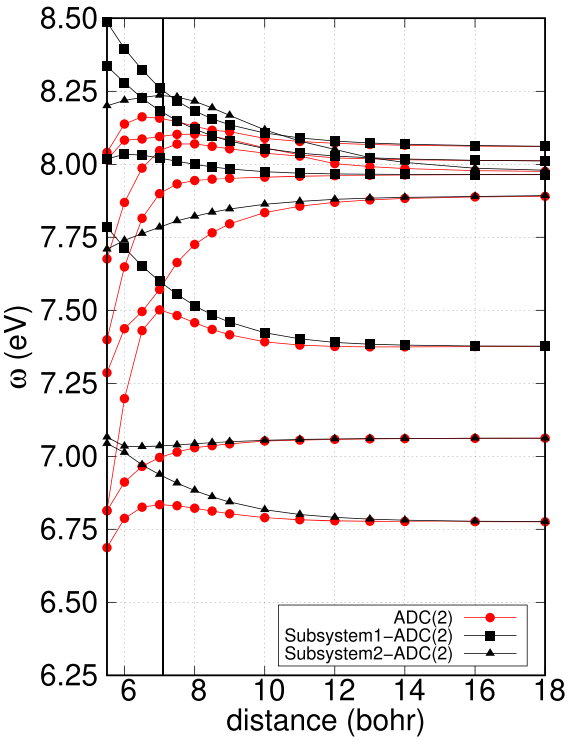


Figure 2. First eight excitation energies of the ethylene−TFE system with respect to the distance between ethylene and TFE for a conventional calculation as compared to the corresponding excitations with the subsystem-ADC(2) approach, both employing a supermolecular basis. A vertical bar is shown at 7.086 bohr.

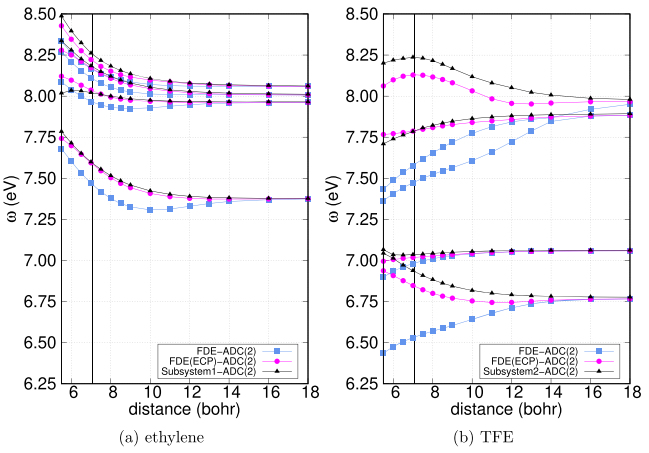


Figure 3. Excitation energies of the subsystems within the ethylene−TFE system with respect to the distance between both subsystems for FDE, FDE(ECP), and subsystem-ADC(2). A vertical bar is shown at 7.086 bohr.

subsystem-ADC(2) as the reference. This figure shows that for long distances the FDE results converge for all states to the subsystem-ADC(2) result, corresponding to a vanishing embedding potential without artifacts in the long-range region.

For most excitations on ethylene, see Figure 3a, the FDE curves are in good agreement with those from subsystem-ADC(2), including intermediate and short distances. However, for the first and the fifth excited states, FDE yields too low of excitation energies for intermediate distances at about 10−12 bohr (curves with boxes). Adding the pseudopotentials to the embedding potential, that is, using FDE(ECP), leads to major improvements for the problematic cases (curves with circles), although FDE(ECP) is not able to provide in all cases accurate shifts for short distances below 7.086 bohr in all cases. In these cases, exchange effects that cannot be captured in the FDE scheme and modeled only very roughly by the ECPs are most likely the reason. The significant improvements when going from FDE to FDE(ECP) support the analysis that the strong attraction is not completely compensated by the kinetic energy functional and the description can be improved using simple pseudopotentials, although at short distances some deviations with respect to the reference subsystem-ADC(2) show up due to remaining errors in the description of Pauli repulsion and exchange effects.

In case of the TFE subsystem of the ethylene−TFE dimer, Figure 3b reveals even more severe problems for the conventional FDE approach. For most of the excitations, significant deviations are obtained between FDE (curve with boxes) and subsystem-ADC(2) (curve with triangles) at distances below 10−12 bohr. For all excited states in this case, excitation energies obtained with the conventional FDE approach decrease with shorter distances, while for some states the subsystem-ADC(2) reference results in an increase, yielding a qualitatively wrong behavior with conventional FDE. To give an example, in case of the fourth excitation, the FDE curve (circles) deviates already clearly from the reference value at a distance as large as 16 bohr. Adding the pseudopotentials to the embedding potential improves the excitation energies significantly. The results are not as close to the subsystem-ADC(2) reference as for the ethylene subsystem but reproduce in all cases the correct behavior of the excitation energies as a function of the distance between the two molecules.

To summarize, the results for the ethylene−TFE dimer reveal unambiguously that simple pseudopotentials increase the accuracy of the numerical outcome of FDE calculations for excitation energies significantly, especially for shorter distances, that is, stronger interactions. In particular, qualitatively wrong curves are corrected to yield a qualitatively correct description.

4.2. Embedding Test Set. Having assessed the accuracy of the FDE(ECP) method as the example of a model dimer system, we now turn to larger systems collected in the test set; see Figure 1. In the left graph of Figure 4, the deviations of the excitation energies ω obtained with FDE-ADC(2) from the subsystem-ADC(2) reference results are shown for the cc-pVTZ and aug-cc-pVTZ basis sets. The corresponding deviations for FDE(ECP)-ADC(2) are shown in the right graph of Figure 4; see also Table 1.

Figure 4 reveals that in case of the cc-pVTZ basis, which does not contain diffuse functions, the deviations are in most cases rather small. The largest deviation is 0.20 eV, and the mean absolute deviation (MAD) is as small as 0.05 eV. Introducing ECPs, the largest deviation decreases slightly to 0.19 eV, and the MAD increases to 0.06 eV. One can conclude that, in this case, the basis set without diffuse functions is not able to allow for excitations into the problematic regions of the environment so that ECPs are not required.

For the aug-cc-pVTZ basis, which contains diffuse functions, Figure 4 reveals an increased MAD of 0.27 eV and a maximum error as large as 1.84 eV. It should be pointed out that the FDE-ADC(2) method consistently underestimates all vertical transition energies resulting in a mean signed deviation (MSD) of −0.27 eV. This indicates an electron spill-out in these systems in case of conventional FDE-ADC(2). Introducing

https://doi.org/10.1021/acs.jctc.1c00732
J. Chem. Theory Comput. 2022, 18, 1737−1747

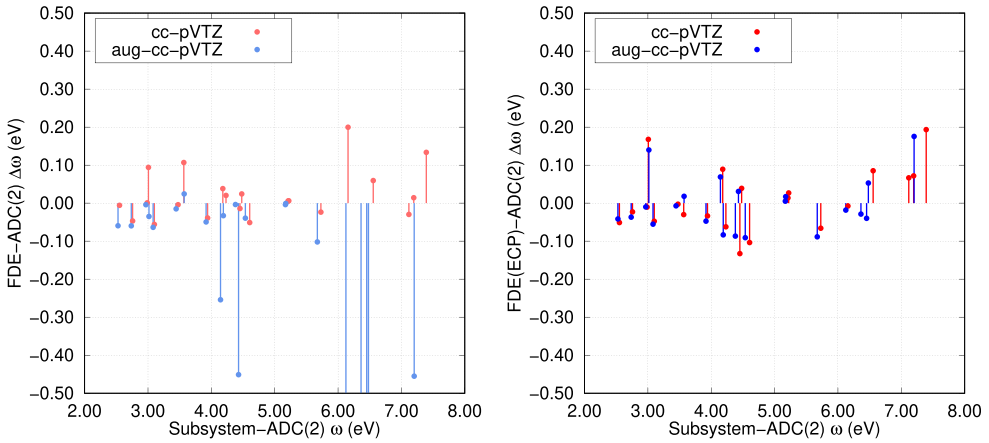


Figure 4. Deviations of the FDE-ADC(2) (left) and FDE(ECP)-ADC(2) (right) excitation energies ($\Delta\omega$) with respect to subsystem-ADC(2) excitation energies ω. Statistics for these deviations are collected in Table 1.

Table 1. Mean Signed Deviation (MSD), Mean Absolute Deviation (MAD), and Maximum Deviation (MAX) for FDE and FDE(ECP) with Respect to Subsystem-ADC(2)[a]

basis	method	MSD	MAD	MAX
cc-pVTZ	FDE-ADC(2)	+0.02	0.05	+0.20
	FDE(ECP)-ADC(2)	< +0.01	0.06	+0.19
aug-cc-pVTZ	FDE-ADC(2)	−0.27	0.27	−1.84
	FDE(ECP)-ADC(2)	> −0.01	0.05	+0.18

[a]See Figure 4. All values are in electronvolts.

ECPs, the largest deviation decreases significantly to 0.18 eV and the MAD to 0.05 eV. The magnitude of the MSD is now reduced below 0.01 eV, showing that the excitation energies are both underestimated and overestimated to a similar amount.

The impact of the ECPs on the physics of the transitions can be illustrated with natural transition orbitals (NTOs). As an example, the occupied and virtual NTOs of the second excitation of system (i) are displayed in Figure 5. The corresponding excitation energy exhibits an error of −1.42 eV in case of FDE-ADC(2) and is reduced to −0.02 eV in case of FDE(ECP)-ADC(2), making it the excitation with the largest influence of the ECPs in our test set. Figure 5 shows that the occupied NTOs differ without and with ECPs and only with ECPs is the correct NTO described, but in both cases they are well localized on the target chromophore. In case of the virtual NTOs, however, the huge influence of the ECPs is revealed. Using FDE-ADC(2) leads to a virtual NTO that is not located on the chromophore but on the environment. By virtue of the ECPs in FDE(ECP)-ADC(2), the virtual NTO is fully (re)located on the chromophore.

To analyze the influence of the ECPs upon the occupied and virtual space, one can compare the frontier orbital energies, that is, the energy of the highest occupied molecular orbital (HOMO) and the lowest unoccupied molecular orbital (LUMO), of FDE-HF and FDE(ECP)-HF. The comparison, see the Supporting Information for details, shows that in most

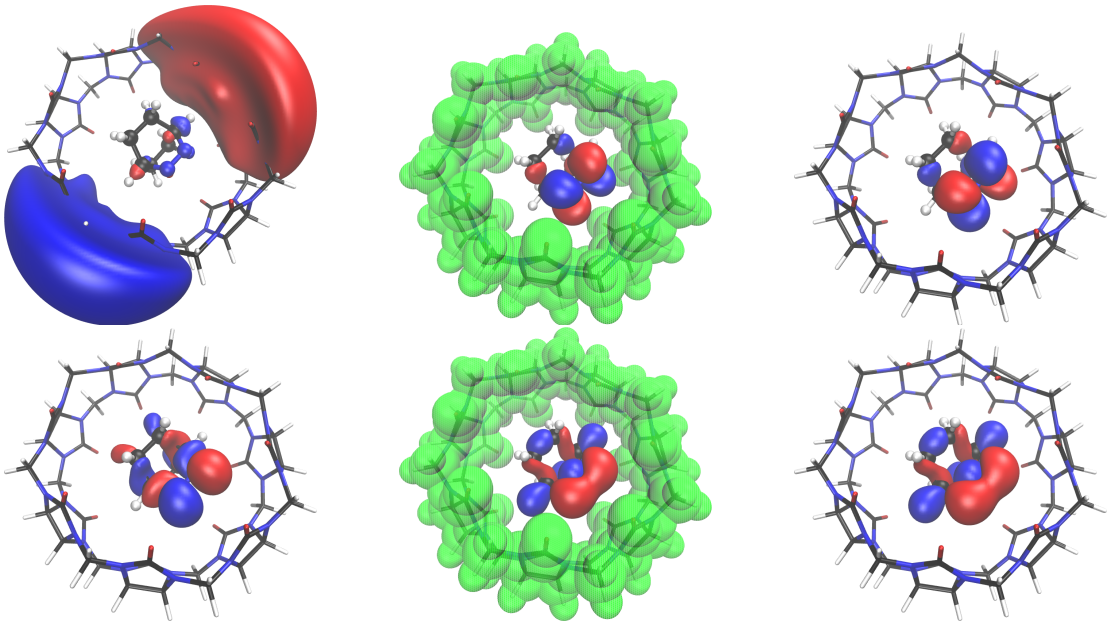


Figure 5. Natural-transition orbitals (NTOs) of the second vertical excitation of system (i). Top, virtual NTOs; bottom, occupied NTOs. Left, FDE method without ECPs; middle, FDE(ECP) method with ECPs displayed in green; right, subsystem-ADC(2).

https://doi.org/10.1021/acs.jctc.1c00732
J. Chem. Theory Comput. 2022, 18, 1737−1747

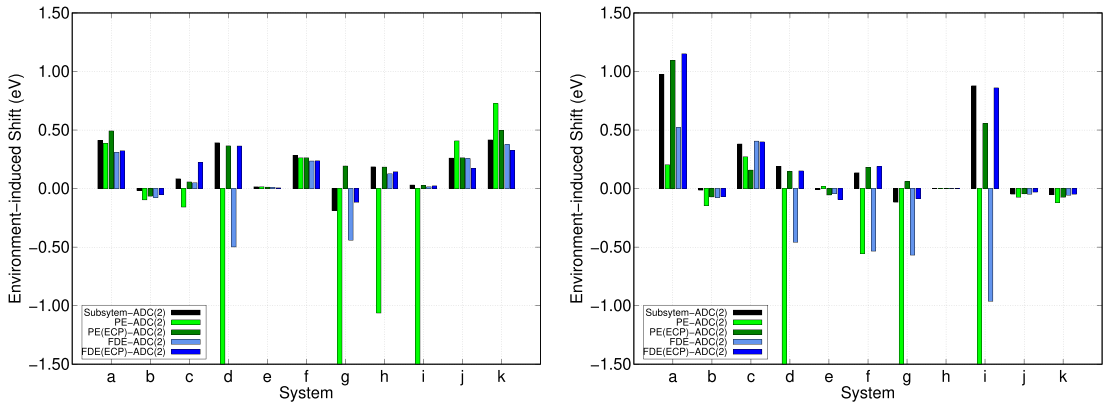


Figure 6. Environment-induced shifts of the first (left) and second (right) vertical excitation energies employing the aug-cc-pVTZ basis set. The PE-ADC(2) and PE(ECP)-ADC(2) excitation energies of systems (a)−(i) are taken from ref 39.

cases the orbital energies increase due to ECPs, which is to be expected due to the additional repulsive term. Only in one case of the test set (system (b)) are lower orbital energies obtained. However, in most cases, the increase in orbital energy is pronounced for the LUMO and in case of diffuse basis functions, while there are only a few cases in which the energy of the HOMO is increased more than the energy of the LUMO.

To give an example, the largest difference between the FDE-ADC(2) and FDE(ECP)-ADC(2) excitation energies occurs in case of system (i). In this case, the HOMO energy is in the cc-pVDZ basis set increased by 47 meV and the LUMO energy by 125 meV, while in the aug-cc-pVTZ, which contains diffuse functions, the HOMO energy is increased by 44 meV and that of the LUMO by 3291 meV.

Figure 6 shows a comparison between the frozen density embedding and the polarizable embedding (both within the frozen solvent approximation) for the environment-induced shifts in the excitation energies in the aug-cc-pVTZ basis. Comparing FDE-ADC(2) and PE-ADC(2), that is, embedding methods without pseudopotentials, reveals that for FDE the electron spill-out problem is not as large as for PE. It is even removed almost entirely for the first excitations of system (i) and (h), but still for FDE many shifts show the wrong sign, revealing that the nonadditive kinetic energy term is in many cases not repulsive enough to repel leaking electrons. However, both embedding methods employing ECPs, that is, FDE(ECP) and PE(ECP), are similarly accurate for the cases investigated in the present work. Employing the same ECPs, FDE(ECP) differs from PE(ECP) in the frozen solvent approximation mainly by the additional nonadditive functional contributions. If ECPs and the nonadditive kinetic contribution lead to a double counting of repulsive effects, an increase of the deviations from the reference values from PE(ECP) to FDE(ECP) would result, but this is not observed in the present work. This leads us to the conclusion that the Pauli repulsion originating from the orthogonality of MOs is described exclusively by the ECPs, which via projection operators shift that part of the Hilbert space that is (in the total supersystem) occupied by the electrons of the environment energetically up so that they are no longer accessible for the electrons of the active subsystem. On the other hand, there is no indication for a significant overestimation of repulsive exchange and kinetic energy contributions for those parts of the Hilbert space not occupied by the electrons of the environment by including both the local ν^i_{kxc} and the nonlocal $\hat{\nu}^i_{\mathrm{ECP}}$ potentials, in the Hamiltonian and Fock operators for the active subsystem.

5. CONCLUSION

In frozen density embedding, available kinetic energy functionals are often not repulsive enough to compensate the nuclear attraction, in particular in regions close to the nuclei. While in ground-state calculations, the missing repulsion does usually not cause problems, it becomes more visible for excited states if the basis set contains diffuse atomic orbitals that are often essential to obtain accurate excitation energies. In the present work, we have proposed an FDE(ECP) scheme in which effective core potentials are included in the embedding potential to account for the missing repulsion. The ECPs do not lead to a significant change in the occupied orbitals but have a significant impact mainly on the virtual orbitals, which are repelled by the ECPs from those parts of the Hilbert space that would be occupied by the electrons of the environment.

The calculations for the ethylene−TFE dimer at different distances revealed that conventional FDE can lead to a qualitatively wrong behavior for several excited states. Employing ECPs in the FDE(ECP) approach leads to a significant improvement, and the qualitative trend of all excited states is reproduced.

For a test set consisting of 11 systems, which are sensitive to electron spill-out, the mean absolute deviation (MAD) for the results in the aug-cc-pVTZ basis set is reduced from 0.27 to 0.05 eV and the maximum error from 1.84 to 0.18 eV when using FDE(ECP) instead of FDE.

The ECPs for bromine and iodine reported in the present work are designed in such a way that they can be used for all p-block elements within the same period. Further improvements could possibly be obtained by using additional functions and parameters in the ECP or by fitting the potentials individually for each element within a period.

Overall, the results from the present work demonstrate that FDE provides a somewhat more robust approximation for the embedding potential with a reduced unphysical electron spill-out than a PE approach with a multipolar representation of the environment's charge density. Also, FDE does not require the parametrization of static and induced multipole moments, which can be another limiting factor for the accuracy of PE models, and it accounts, in difference to the latter, also for nonadditive kinetic, exchange, and correlation contributions. However, the remaining errors in FDE due to the approximate

https://doi.org/10.1021/acs.jctc.1c00732
J. Chem. Theory Comput. 2022, 18, 1737−1747

account of repulsive contributions by the kinetic energy functionals can still be sizable and can limit the accuracy of the excitation energies, in particular for diffuse basis functions. Incorporating in the FDE calculations the same simple ECPs as proposed recently for PE leads to significantly improved excitation energies. A double counting of repulsive contributions that could be anticipated when ECPs are included, in addition to the nonadditive kinetic energy contributions, is not observed.

■ ASSOCIATED CONTENT

Supporting Information

The Supporting Information is available free of charge at https://pubs.acs.org/doi/10.1021/acs.jctc.1c00732.

ECP parameters, orbital energy differences between FDE and FDE(ECP), calculated excitation energies, comparison of localization, comparison of kinetic functionals, and comparison with long distance correction (PDF)

■ AUTHOR INFORMATION

Corresponding Authors

Robert S. Treß − *Department of Theoretical Chemistry, Ruhr University Bochum, Bochum 44801, Germany;* orcid.org/0000-0001-8804-3547; Email: robert.tress@rub.de

Sebastian Höfener − *Institute of Physical Chemistry, Karlsruhe Institute of Technology (KIT), Karlsruhe 76131, Germany;* orcid.org/0000-0003-4504-347X; Email: hoefener@kit.edu

Author

Christof Hättig − *Department of Theoretical Chemistry, Ruhr University Bochum, Bochum 44801, Germany;* orcid.org/0000-0002-5752-2710

Complete contact information is available at: https://pubs.acs.org/10.1021/acs.jctc.1c00732

Notes

The authors declare no competing financial interest.

■ ACKNOWLEDGMENTS

We thank TURBOMOLE GmbH for funding. C.H. acknowledges support by the Deutsche Forschungsgemeinschaft with the Priority Program SPP 1807 (HA 25888/10-1). S.H. acknowledges support by the Deutsche Forschungsgemeinschaft through SFB 1249 "N-Heteropolycycles as Functional Materials" (project B07).

■ REFERENCES

(1) Warshel, A.; Levitt, M. Theoretical studies of enzymic reactions: dielectric, electrostatic and steric stabilization of the carbonium ion in the reaction of lysozyme. *J. Mol. Biol.* **1976**, *103*, 227−249.

(2) Senn, H. M.; Thiel, W. QM/MM methods for biomolecular systems. *Angew. Chem., Int. Ed.* **2009**, *48*, 1198−1229.

(3) Brunk, E.; Rothlisberger, U. Mixed quantum mechanical/molecular mechanical molecular dynamics simulations of biological systems in ground and electronically excited states. *Chem. Rev.* **2015**, *115*, 6217−6263.

(4) List, N. H.; Olsen, J. M. H.; Kongsted, J. Excited states in large molecular systems through polarizable embedding. *Phys. Chem. Chem. Phys.* **2016**, *18*, 20234−20250.

(5) Morzan, U. N.; Alonso de Armino, D. J.; Foglia, N. O.; Ramirez, F.; Gonzalez Lebrero, M. C.; Scherlis, D. A.; Estrin, D. A. Spectroscopy in complex environments from QM-MM simulations. *Chem. Rev.* **2018**, *118*, 4071−4113.

(6) Olsen, J. M.; Aidas, K.; Kongsted, J. Excited states in solution through polarizable embedding. *J. Chem. Theory Comput.* **2010**, *6*, 3721−3734.

(7) Wesolowski, T. A.; Warshel, A. Frozen density functional approach for ab initio calculations of solvated molecules. *J. Phys. Chem.* **1993**, *97*, 8050−8053.

(8) Govind, N.; Wang, Y.; Da Silva, A.; Carter, E. Accurate ab initio energetics of extended systems via explicit correlation embedded in a density functional environment. *Chem. Phys. Lett.* **1998**, *295*, 129−134.

(9) Govind, N.; Wang, Y. A.; Carter, E. A. Electronic-structure calculations by first-principles density-based embedding of explicitly correlated systems. *J. Chem. Phys.* **1999**, *110*, 7677−7688.

(10) Gomes, A. S. P.; Jacob, C. R.; Visscher, L. Calculation of local excitations in large systems by embedding wave-function theory in density-functional theory. *Phys. Chem. Chem. Phys.* **2008**, *10*, 5353−5362.

(11) Höfener, S.; Severo Pereira Gomes, A.; Visscher, L. Molecular properties via a subsystem density functional theory formulation: A common framework for electronic embedding. *J. Chem. Phys.* **2012**, *136*, 044104.

(12) Prager, S.; Zech, A.; Aquilante, F.; Dreuw, A.; Wesolowski, T. A. First time combination of frozen density embedding theory with the algebraic diagrammatic construction scheme for the polarization propagator of second order. *J. Chem. Theory Comput.* **2016**, *144*, 204103.

(13) Prager, S.; Zech, A.; Wesolowski, T. A.; Dreuw, A. Implementation and application of the frozen density embedding theory with the algebraic diagrammatic construction scheme for the polarization propagator up to third order. *J. Chem. Theory Comput.* **2017**, *13*, 4711−4725.

(14) Daday, C.; König, C.; Neugebauer, J.; Filippi, C. Wavefunction in density functional theory embedding for excited states: Which wavefunctions, which densities? *ChemPhysChem* **2014**, *15*, 3205−3217.

(15) Casida, M. E.; Wesolowski, T. A. Generalization of the Kohn-Sham equations with constrained electron density formalism and its time-dependent response theory formulation. *Int. J. Quantum Chem.* **2004**, *96*, 577−588.

(16) Neugebauer, J. Couplings between electronic transitions in a subsystem formulation of time-dependent density functional theory. *J. Chem. Phys.* **2007**, *126*, 134116.

(17) Neugebauer, J. On the calculation of general response properties in subsystem density functional theory. *J. Chem. Phys.* **2009**, *131*, 084104.

(18) Kristyán, S.; Pulay, P. Can (semi) local density functional theory account for the London dispersion forces? *Chem. Phys. Lett.* **1994**, *229*, 175−180.

(19) Stefanovich, E. V.; Truong, T. N. Embedded density functional approach for calculations of adsorption on ionic crystals. *J. Chem. Phys.* **1996**, *104*, 2946−2955.

(20) Jacob, C. R.; Wesolowski, T. A.; Visscher, L. Orbital-free embedding applied to the calculation of induced dipole moments in CO2···X (X = He, Ne, Ar, Kr, Xe, Hg) van der Waals complexes. *J. Chem. Phys.* **2005**, *123*, 174104.

(21) Dułak, M.; Wesolowski, T. A. On the electron leak problem in orbital-free embedding calculations. *J. Chem. Phys.* **2006**, *124*, 164101.

(22) Fradelos, G.; Wesolowski, T. A. Importance of the Intermolecular Pauli Repulsion in Embedding Calculations for Molecular Properties: The Case of Excitation Energies for a Chromophore in Hydrogen-Bonded Environments. *J. Phys. Chem. A* **2011**, *115*, 10018−10026.

(23) Zech, A.; Ricardi, N.; Prager, S.; Dreuw, A.; Wesolowski, T. A. Benchmark of excitation energy shifts from frozen-density embedding theory: introduction of a density-overlap-based applicability threshold. *J. Chem. Theory Comput.* **2018**, *14*, 4028−4040.

(24) Jacob, C. R.; Beyhan, S. M.; Visscher, L. Exact functional derivative of the nonadditive kinetic-energy bifunctional in the long-distance limit. *J. Chem. Phys.* **2007**, *126*, 234116.
(25) Schlüns, D.; Klahr, K.; Mück-Lichtenfeld, C.; Visscher, L.; Neugebauer, J. Subsystem-DFT potential-energy curves for weakly interacting systems. *Phys. Chem. Chem. Phys.* **2015**, *17*, 14323−14341.
(26) Grimme, S. Accurate description of van der Waals complexes by density functional theory including empirical corrections. *J. Comput. Chem.* **2004**, *25*, 1463−1473.
(27) Grimme, S.; Antony, J.; Ehrlich, S.; Krieg, H. A consistent and accurate ab initio parametrization of density functional dispersion correction (DFT-D) for the 94 elements H-Pu. *J. Chem. Phys.* **2010**, *132*, 154104.
(28) Chulhai, D. V.; Jensen, L. Frozen Density Embedding with External Orthogonality in Delocalized Covalent Systems. *J. Chem. Theory Comput.* **2015**, *11*, 3080−3088.
(29) Manby, F. R.; Stella, M.; Goodpaster, J. D.; Miller, T. F., III A simple, exact density-functional-theory embedding scheme. *J. Chem. Theory Comput.* **2012**, *8*, 2564−2568.
(30) Goodpaster, J. D.; Barnes, T. A.; Manby, F. R.; Miller, T. F., III Accurate and systematically improvable density functional theory embedding for correlated wavefunctions. *J. Chem. Phys.* **2014**, *140*, 18A507.
(31) Barnes, T. A.; Goodpaster, J. D.; Manby, F. R.; Miller, T. F., III Accurate basis set truncation for wavefunction embedding. *J. Chem. Phys.* **2013**, *139*, 024103.
(32) Chulhai, D. V.; Jensen, L. External orthogonality in subsystem time-dependent density functional theory. *Phys. Chem. Chem. Phys.* **2016**, *18*, 21032−21039.
(33) Tölle, J.; Böckers, M.; Neugebauer, J. Exact subsystem time-dependent density-functional theory. *J. Chem. Phys.* **2019**, *150*, 181101.
(34) Niemeyer, N.; Tölle, J.; Neugebauer, J. Approximate versus Exact Embedding for Chiroptical Properties: Reconsidering Failures in Potential and Response. *J. Chem. Theory Comput.* **2020**, *16*, 3104−3120.
(35) Scholz, L.; Tölle, J.; Neugebauer, J. Analysis of environment response effects on excitation energies within subsystem-based time-dependent density-functional theory. *Int. J. Quantum Chem.* **2020**, *120*, e26213.
(36) Tölle, J.; Böckers, M.; Niemeyer, N.; Neugebauer, J. Inter-subsystem charge-transfer excitations in exact subsystem time-dependent density-functional theory. *J. Chem. Phys.* **2019**, *151*, 174109.
(37) Fux, S.; Jacob, C. R.; Neugebauer, J.; Visscher, L.; Reiher, M. Accurate frozen-density embedding potentials as a first step towards a subsystem description of covalent bonds. *J. Chem. Phys.* **2010**, *132*, 164101.
(38) Artiukhin, D. G.; Jacob, C. R.; Neugebauer, J. Excitation energies from frozen-density embedding with accurate embedding potentials. *J. Chem. Phys.* **2015**, *142*, 234101.
(39) Marefat Khah, A.; Reinholdt, P.; Olsen, J. M. H.; Kongsted, J.; Hättig, C. Avoiding electron spill-out in QM/MM calculations on excited states with simple pseudopotentials. *J. Chem. Theory Comput.* **2020**, *16*, 1373−1381.
(40) Schirmer, J. Beyond the random-phase approximation: A new approximation scheme for the polarization propagator. *Phys. Rev. A* **1982**, *26*, 2395.
(41) Trofimov, A.; Schirmer, J. An efficient polarization propagator approach to valence electron excitation spectra. *J. Phys. B: At. Mol. Opt. Phys.* **1995**, *28*, 2299.
(42) Schirmer, J.; Trofimov, A. Intermediate state representation approach to physical properties of electronically excited molecules. *J. Chem. Phys.* **2004**, *120*, 11449−11464.
(43) Dolg, M.; Cao, X. Relativistic pseudopotentials: their development and scope of applications. *Chem. Rev.* **2012**, *112*, 403−480.
(44) Luaña, V.; Pueyo, L. Simulation of ionic crystals: The ab initio perturbed-ion method and application to alkali hydrides and halides. *Phys. Rev. B* **1990**, *41*, 3800.
(45) Barandiarán, Z.; Seijo, L. The ab initio model potential representation of the crystalline environment. theoretical study of the local distortion on NaCl: Cu+. *J. Chem. Phys.* **1988**, *89*, 5739−5746.
(46) Swerts, B.; Chibotaru, L. F.; Lindh, R.; Seijo, L.; Barandiaran, Z.; Clima, S.; Pierloot, K.; Hendrickx, M. F. Embedding fragment ab initio model potentials in CASSCF/CASPT2 calculations of doped solids: implementation and applications. *J. Chem. Theory Comput.* **2008**, *4*, 586−594.
(47) von Lilienfeld, O. A.; Tavernelli, I.; Rothlisberger, U.; Sebastiani, D. Variational optimization of effective atom centered potentials for molecular properties. *J. Chem. Phys.* **2005**, *122*, 014113.
(48) Zhang, Y.; Lee, T.-S.; Yang, W. A pseudobond approach to combining quantum mechanical and molecular mechanical methods. *J. Chem. Phys.* **1999**, *110*, 46−54.
(49) Slavíček, P.; Martínez, T. J. Multicentered valence electron effective potentials: A solution to the link atom problem for ground and excited electronic states. *J. Chem. Phys.* **2006**, *124*, 084107.
(50) DiLabio, G. A.; Hurley, M. M.; Christiansen, P. A. Simple one-electron quantum capping potentials for use in hybrid QM/MM studies of biological molecules. *J. Chem. Phys.* **2002**, *116*, 9578−9584.
(51) Corni, S.; Cammi, R.; Mennucci, B.; Tomasi, J. Electronic excitation energies of molecules in solution within continuum solvation models: Investigating the discrepancy between state-specific and linear-response methods. *J. Chem. Phys.* **2005**, *123*, 134512.
(52) Valle, F. J. O. D.; Tomasi, J. Electron correlation and solvation effects. I. Basic formulation and preliminary attempt to include the electron correlation in the quantum mechanical polarizable continuum model so as to study solvation phenomena. *Chem. Phys.* **1991**, *150*, 139−150.
(53) Hopffgarten, M. v.; Frenking, G. Energy decomposition analysis. *Wiley Interdiscip. Rev.: Comput. Mol. Sci.* **2012**, *2*, 43−62.
(54) Jacob, C. R.; Neugebauer, J. Subsystem density-functional theory. *Wiley Interdiscip. Rev.: Comput. Mol. Sci.* **2014**, *4*, 325−362.
(55) Helmich, B.; Hättig, C. A pair natural orbital implementation of the coupled cluster model CC2 for excitation energies. *J. Chem. Phys.* **2013**, *139*, 084114.
(56) Development version of TURBOMOLE 2019, a development of the University of Karlsruhe and Forschungszentrum Karlsruhe GmbH, 1989−2007, TURBOMOLE GmbH, since 2007; available from http://www.turbomole.com (accessed Apr 23, 2021).
(57) Perdew, J. P.; Burke, K.; Ernzerhof, M. Generalized gradient approximation made simple. *Phys. Rev. Lett.* **1996**, *77*, 3865.
(58) Lembarki, A.; Chermette, H. Obtaining a gradient-corrected kinetic-energy functional from the Perdew-Wang exchange functional. *Phys. Rev. A* **1994**, *50*, 5328.
(59) Becke, A. D. Density-functional thermochemistry. I. The effect of the exchange-only gradient correction. *J. Chem. Phys.* **1992**, *96*, 2155−2160.
(60) Woon, D. E.; Dunning, T. H. Gaussian basis sets for use in correlated molecular calculations. IV. Calculation of static electrical response properties. *J. Chem. Phys.* **1994**, *100*, 2975−2988.
(61) Dunning, T. H. Gaussian basis sets for use in correlated molecular calculations. I. The atoms boron through neon and hydrogen. *J. Chem. Phys.* **1989**, *90*, 1007−1023.
(62) Kendall, R. A.; Dunning, T. H.; Harrison, R. J. Electron affinities of the first-row atoms revisited. Systematic basis sets and wave functions. *J. Chem. Phys.* **1992**, *96*, 6796−6806.
(63) Laricchia, S.; Fabiano, E.; Constantin, L.; Della Sala, F. Generalized gradient approximations of the noninteracting kinetic energy from the semiclassical atom theory: Rationalization of the accuracy of the frozen density embedding theory for nonbonded interactions. *J. Chem. Theory Comput.* **2011**, *7*, 2439−2451.
(64) Thomas, L. H. The calculation of atomic fields. *Math. Proc. Camb. Philos. Soc.* **1927**, *23*, 542−548.
(65) Fermi, E. Statistical method to determine some properties of atoms. *Rend. Accad. Naz. Lincei* **1927**, *6*, 5.

https://doi.org/10.1021/acs.jctc.1c00732
J. Chem. Theory Comput. 2022, 18, 1737−1747

(66) Boys, S. F. Construction of some molecular orbitals to be approximately invariant for changes from one molecule to another. *Rev. Mod. Phys.* **1960**, *32*, 296.
(67) Foster, J.; Boys, S. Canonical configurational interaction procedure. *Rev. Mod. Phys.* **1960**, *32*, 300.
(68) Jansík, B.; Høst, S.; Kristensen, K.; Jørgensen, P. Local orbitals by minimizing powers of the orbital variance. *J. Chem. Phys.* **2011**, *134*, 194104.
(69) Høyvik, I.-M.; Jansik, B.; Jørgensen, P. Orbital localization using fourth central moment minimization. *J. Chem. Phys.* **2012**, *137*, 224114.

Recommended by ACS

Applying Generalized Variational Principles to Excited-State-Specific Complete Active Space Self-consistent Field Theory

Rebecca Hanscam and Eric Neuscamman
OCTOBER 10, 2022
JOURNAL OF CHEMICAL THEORY AND COMPUTATION
READ

Explicitly Correlated Electronic Structure Calculations with Transcorrelated Matrix Product Operators

Alberto Baiardi, Markus Reiher, *et al.*
JUNE 06, 2022
JOURNAL OF CHEMICAL THEORY AND COMPUTATION
READ

General, Rigorous Approach for the Treatment of Interfragment Covalent Bonds

Bryce M. Westheimer and Mark S. Gordon
SEPTEMBER 27, 2022
THE JOURNAL OF PHYSICAL CHEMISTRY A
READ

Koopmans Spectral Functionals in Periodic Boundary Conditions

Nicola Colonna, Nicola Marzari, *et al.*
AUGUST 04, 2022
JOURNAL OF CHEMICAL THEORY AND COMPUTATION
READ

Get More Suggestions >

https://doi.org/10.1021/acs.jctc.1c00732
J. Chem. Theory Comput. 2022, 18, 1737−1747